

~~CONFIDENTIAL~~

NACA RM L56D13

7691

NACA

Ry # 6039
JUL 17 1956

DL44159



TECH LIBRARY KAFB, NM

RESEARCH MEMORANDUM

SOME EFFECTS OF WING FENCES ON THE LATERAL STABILITY
DERIVATIVES OF A 60° DELTA WING OSCILLATING
CONTINUOUSLY IN YAW

By Donald R. Riley

Langley Aeronautical Laboratory
Langley Field, Va.

~~CONFIDENTIAL~~

NATIONAL ADVISORY COMMITTEE FOR AERONAUTICS

WASHINGTON

July 11, 1956

~~CONFIDENTIAL~~



NATIONAL ADVISORY COMMITTEE FOR AERONAUTICS

RESEARCH MEMORANDUM

SOME EFFECTS OF WING FENCES ON THE LATERAL STABILITY

DERIVATIVES OF A 60° DELTA WING OSCILLATING

CONTINUOUSLY IN YAW

By Donald R. Riley

SUMMARY

An investigation at low speed has been conducted in the Langley stability tunnel to determine some of the effects of wing fences on the lateral stability derivatives of a flat-plate 60° delta-wing model oscillating continuously in yaw. Results were obtained for the rolling-moment and yawing-moment derivatives in phase and out of phase with the model motion.

The results indicated that the addition of wing fences provided large reductions in the magnitudes of the damping-in-yaw and cross (rolling moment due to yawing) derivatives at high angles of attack and low reduced frequency by reducing the amount of separated flow on the wing surface. Corresponding increases were obtained in the magnitude of the in-phase derivatives, the directional stability and effective dihedral. Increases in Reynolds number and the use of various devices commonly employed to improve the longitudinal stability characteristics by reducing flow separation such as camber, twist, and leading-edge flaps and slats may provide changes in the oscillatory derivatives similar to the changes produced by wing fences.

INTRODUCTION

A number of recent wind-tunnel investigations have shown that, for unsteady motion, large values of some of the lateral stability derivatives exist at moderate and high angles of attack for swept and delta plan-form wings. Results presented in references 1 to 4 indicate that the large values of the derivatives are associated with the separated flow on the wing surface that results primarily from wing sweep. Since wing fences, which have been employed to improve the longitudinal characteristics of swept and delta wings, alter the flow condition on the wing, the possibility exists that these devices also affect the unsteady values of the lateral stability derivatives.

1718

The present investigation was undertaken to determine some of the effects of wing fences on the unsteady values of the lateral stability derivatives of a 60° delta-wing model. The tests consisted of measuring the yawing and rolling moments when the model was oscillating continuously in yaw about its vertical wind axis. Since the model motion is a combination of yawing and sideslipping, the stability derivatives measured by this technique are combination derivatives. These derivatives are the damping in yaw $C_{n_r, \omega} - C_{n\dot{\beta}, \omega}$, the cross derivative (rolling moment due to yawing) $C_{l_r, \omega} - C_{l\dot{\beta}, \omega}$, the directional stability $C_{n_{\beta}, \omega} + k^2 C_{n\dot{r}, \omega}$, and the effective dihedral derivative $C_{l_{\beta}, \omega} + k^2 C_{l\dot{r}, \omega}$, where k in the expressions is the reduced-frequency parameter $\omega b/2V$. The damping-in-yaw and cross derivatives were obtained from moment components out of phase with the model motion. In-phase moment components provided the directional stability and effective dihedral derivatives. The results presented show some of the effects of fence geometric characteristics, frequency of oscillation, oscillation amplitude, and angle of attack.

SYMBOLS

The data presented herein are in the form of stability derivatives and moment coefficients which are referred to the stability system of axes with the origin located at the quarter-chord point of the mean aerodynamic chord projected on the plane of symmetry. The positive directions of moments and angles are shown in figure 1. The derivatives, coefficients, and symbols are defined as follows:

C_n	yawing-moment coefficient, $\frac{\text{Yawing moment}}{qSb}$
C_l	rolling-moment coefficient, $\frac{\text{Rolling moment}}{qSb}$
S	wing area, sq ft
b	wing span, ft
q	dynamic pressure, lb/sq ft, $\frac{1}{2}\rho V^2$
ρ	mass density of air, slugs/cu ft
V	free-stream velocity, fps
α	angle of attack, deg

~~CONFIDENTIAL~~

β	angle of sideslip, radians or degrees
$\dot{\beta}$	rate of change of angle of sideslip with time, radians/sec
ψ	angle of yaw, radians or deg
ψ_0	amplitude of yaw, deg
r	angular velocity in yaw ($r = \dot{\psi}$), radians/sec
\dot{r}	rate of change of angular velocity in yaw with time ($\dot{r} = \ddot{\psi}$)
k	reduced-frequency parameter, $\omega b/2V$
ω	circular frequency of oscillation, radians/sec
f	frequency of oscillation, cps
X	fence chordwise length measured from wing leading edge, in.
c	wing chord, ft
y	fence spanwise location measured from plane of symmetry, ft
h	fence height above wing surface, in.
t	maximum wing thickness, in.

$$C_{n\beta} = \frac{\partial C_n}{\partial \beta}$$

$$C_{n\dot{\beta}} = \frac{\partial C_n}{\partial \frac{\dot{\beta} b}{2V}}$$

$$C_{nr} = \frac{\partial C_n}{\partial \frac{rb}{2V}}$$

$$C_{n\dot{r}} = \frac{\partial C_n}{\partial \frac{\dot{r} b^2}{4V^2}}$$

$$C_{l\beta} = \frac{\partial C_l}{\partial \beta}$$

~~CONFIDENTIAL~~

$$C_{l\dot{\beta}} = \frac{\partial C_l}{\partial \frac{\dot{\beta} b}{2V}}$$

$$C_{l_r} = \frac{\partial C_l}{\partial \frac{rb}{2V}}$$

$$C_{l_{\dot{r}}} = \frac{\partial C_l}{\partial \frac{\dot{r} b^2}{4V^2}}$$

All derivatives used in this paper are nondimensionalized (per radian). The symbol $\dot{}$ following the subscript of a derivative denotes the oscillatory derivative.

MODEL AND APPARATUS

Model

The delta wing had a leading-edge sweep angle of 60° and was the same model used in the investigations of references 1, 3, and 4. The wing was constructed from 3/4-inch plywood having essentially a flat-plate airfoil section with a circular leading edge and a beveled trailing edge. The trailing edge was beveled to provide a trailing-edge angle of 10° that was constant across the span. A photograph of the model mounted on the strain-gage balance which in turn was fastened to the oscillation strut is presented as figure 2. The canopy shown in the photograph was made from balsa and served to streamline the protrusion of the strain-gage balance above the upper surface of the wing at angles of attack. All openings in the canopy were sealed to prevent leakage of air through the model. A sketch of the model and its geometric characteristics is presented as figure 3.

The fences used for the present investigation had profiles as shown in figure 4 and were constructed from 0.50-inch-thick brass. Figure 4 also shows the four spanwise fence locations which were used; namely, $0.35b/2$, $0.50b/2$, $0.60b/2$, and $0.70b/2$. The chordwise distances indicated in the figure are the maximum fence lengths X tested at each spanwise station. Fences were made having heights h of $1/4$, $1/2$, and $3/4$ inch. These heights were chosen to provide values of the ratio of fence height to wing thickness of $1/3$, $2/3$, and 1.0 . It should be noted that, for the fence profile used, an increase in height also means an increase in overhang of the fence at the wing leading edge.

A summary of the various wing-fence configurations tested, indicating the geometric characteristics of the fences and their spanwise locations, is presented in table I. In addition, similar information is tabulated on each of the data figures for the particular wing-fence configurations that correspond to the data.

Oscillation Apparatus

The equipment used to oscillate the model was the same equipment used in the investigation of reference 4 and consisted of a motor-driven flywheel, connecting rod, crank arm, and model-support strut. This apparatus is shown schematically in figure 5 and photographically in figure 6. The connecting rod was pinned to an eccentric center on the flywheel and transmitted a sinusoidal yawing motion to the support strut by means of the crank arm. The model was mounted on a strain-gage balance which, in turn, was fastened rigidly to the support strut. Model angle of attack was changed by rotating the model relative to the balance about the quarter-chord position. The apparatus, therefore, produced a forced oscillation about the vertical wind or stability axes. The frequency of oscillation was varied by changing the voltage supplied to the motor, and the oscillation amplitude was varied by adjusting the throw of the eccentric on the flywheel.

Recording of Data

The recording of data was accomplished by means of the equipment described completely in the appendix of reference 3. Briefly, measurement of the rolling and yawing moments acting on the model during oscillation were made by means of resistance-type strain gages which were supplied with voltages obtained from the sine-cosine resolver that was geared directly to the flywheel shaft. The output signals from the strain gages were proportional to the in-phase and out-of-phase components of the moments. Average values of these signals were read visually on a highly damped d-c ammeter. The aerodynamic coefficients were obtained by multiplying the ammeter readings by the appropriate constants, one of which was the system-calibration constant.

TESTS

The investigation was made in the 6- by 6-foot test section of the Langley stability tunnel at a dynamic pressure of 24.9 pounds per square foot which corresponds to a Mach number of 0.13. The Reynolds number based on the wing mean aerodynamic chord was approximately 1.6×10^6 .

For each of the oscillatory test conditions, tests were made both with the fences on and with fences off in order to determine the effect of wing fences on the stability derivatives. For single fence configurations, that is, for one fence located on each semispan of the wing, some of the effects associated with variations in fence geometry, angle of attack, frequency of oscillation, and oscillation amplitude were investigated. Some data were also obtained for the wing with several multiple fence configurations. A summary table for the fence-on oscillation tests indicating the fence configurations and corresponding test conditions is presented as table I.

In addition to the oscillation tests, static-sideslip tests were made at $\alpha = 24^\circ$ for the wing model with two single fence configurations and with fences off. For these tests, the model was mounted on the oscillation strut and data were obtained at increments of 2° over a range of β from -10° to 10° . At a later date, additional static-sideslip data were obtained for the model with the same two single fence configurations and with fences off through the angle-of-attack range at β of -6° and $+6^\circ$ to permit an evaluation of $C_{n\beta}$ and $C_{l\beta}$ with α . For these additional tests, the wing model was mounted on a conventional single strut support with a streamlined fairing present. To provide an indication of the difference in the interference effects of the two supporting systems, data for the latter tests were obtained for the model with fences off every 2° over a range of β from -6° to 6° for an angle of attack of 24° . With fences on, data were recorded at $\alpha = 24^\circ$ for sideslip angles of 6° , 0° , and -6° . All the tests, both oscillatory and static, were made with the canopy on the delta wing.

For the oscillation tests, the in-phase and out-of-phase components of the yawing and rolling moments were measured for each configuration and test condition for both wind-on and wind-off. The effects of the inertia of the model were eliminated from the data by subtracting the wind-off from the wind-on results. Previous experience (see ref. 1, for example), wherein wind-off tests were conducted with the model encased in a plywood box, indicated that still-air aerodynamic inertial effects would not influence the wind-off readings.

CORRECTIONS

The usual jet-boundary corrections to angle of attack have not been applied to the data, because the longitudinal characteristics were not obtained for the fence-on configurations. The lift, drag, and pitching-moment characteristics for the wing with canopy are presented in references 1, 3, and 4 at a somewhat higher dynamic pressure (39.7 pounds per square foot). The resonance effect discussed in reference 5 becomes

important only for the frequencies considered herein at Mach numbers near unity and thus requires no consideration. In addition, the data have not been corrected for blockage or support interference.

RESULTS AND DISCUSSION

Variation With Angle of Attack

Values of the unsteady derivatives for the delta wing with and without a fence on each wing semispan are presented for an angle-of-attack range from 0° to 30° in figure 7 for an oscillation amplitude ψ_0 of $\pm 6^\circ$ and a reduced frequency k of 0.065. Data for the wing with several multiple fence configurations are also shown for the same test conditions at the higher angles of attack ($\alpha = 24^\circ$ to 30°).

The variations of the fence-off results with α are similar to those shown in references 2 and 4. At the high angles of attack, the magnitudes of the damping-in-yaw derivative $C_{n_{r,\omega}} - C_{n_{\dot{\beta},\omega}}$ and cross (rolling moment due to yawing) derivative $C_{l_{r,\omega}} - C_{l_{\dot{\beta},\omega}}$ increase rapidly with α and attain values several times larger than those for complete models operating in the low-angle-of-attack range. These large changes in the values of the derivatives with angle of attack appear to develop in proportion to the degree of flow separation on the wing surface. (See refs. 1 and 2.) The analysis of reference 2 has attributed the large magnitudes of the out-of-phase derivatives to a lag in the alternating increase and decrease in separated flow over the wing panels as the wing oscillates in yaw. The significance of these large magnitude derivatives on dynamic lateral stability is pointed out in reference 6, and some information on the relative importance of the two terms making up the damping-in-yaw and cross derivatives is presented in reference 4.

Comparison of fence-off results with those for a single fence on each wing semispan indicates that, for $C_{n_{r,\omega}} - C_{n_{\dot{\beta},\omega}}$ and $C_{l_{r,\omega}} - C_{l_{\dot{\beta},\omega}}$, the addition of the wing fences reduced the magnitudes of the derivatives at the high angles of attack, but did not change the relatively small values that were obtained at the low angles of attack. This effect apparently resulted from a reduction in the amount of flow separation on the wing surface. Multiple fence configurations appeared to reduce the amount of flow separation even further in that they reduced the magnitudes of the derivatives in the high α range more than did the single fence configuration. Even though the fences reduced the magnitudes of the derivatives at high angles of attack, the general trend of an increase in magnitude with α at the highest angles tested still remains.

Comparisons of the fence-off and fence-on data for the in-phase derivatives indicate that increases in directional stability

$C_{n\beta,\omega} + k^2 C_{n\dot{r},\omega}$ and effective dihedral $C_{l\beta,\omega} + k^2 C_{l\dot{r},\omega}$ were obtained when fences were added, such that the values of the derivatives for the model with fences on more nearly approached the theoretical values for unseparated flow. This fact is rather apparent in the effective dihedral data in that the fences extended the low-angle-of-attack trend to higher values of α . Use of multiple fence configurations provided even further increases in the magnitude of these two derivatives at the higher angles of attack. A comparison of the in-phase derivatives with the out-of-phase derivatives for fences on and off indicates that increases in the in-phase derivatives $C_{n\beta,\omega} + k^2 C_{n\dot{r},\omega}$ and $C_{l\beta,\omega} + k^2 C_{l\dot{r},\omega}$ results in corresponding decreases in the out-of-phase derivatives $C_{n\dot{r},\omega} - C_{n\beta,\omega}$ and $C_{l\dot{r},\omega} - C_{l\beta,\omega}$.

To substantiate the relationship between separated flow and the large magnitudes of the damping-in-yaw and cross derivatives, static-sideslip data were obtained for the delta-wing model with and without fences through the angle-of-attack range. The tests were conducted at $\beta = \pm 6^\circ$, and the results are presented in the form of static-sideslip derivatives in figure 8. The reduction in the rate of increase of $C_{l\beta}$ with α above an angle of attack of about 8° for the delta-wing model with fences off is due to a more extensive amount of flow separation on the leading wing semispan than on the trailing semispan. This fact has been well established for swept wings by a number of surface tuft surveys. (For example, see refs. 7 and 8.) For the angle-of-attack range from 8° to about 16° , the addition of the fences probably eliminated most of the separated flow on the wing as evidenced by the extension of the linear range of $C_{l\beta}$ to a higher angle of attack. For values of α above 16° , the fences were effective in reducing the amount of separated flow and may have provided some stabilization of the flow. (See also ref. 9.) Additional substantiation of the reduction in the amount of separated flow when fences are added is provided by the more linear variation of the rolling- and yawing-moment coefficients with β that were obtained when fences were added to the delta wing (fig. 9). A comparison of the results presented in figures 7 and 8 indicates that the addition of fences provided changes in the in-phase oscillatory derivatives (fig. 7) similar to those shown for the static derivatives $C_{n\beta}$ and $C_{l\beta}$ (fig. 8), and that, as a result, the primary effect of the fence in the oscillatory case was much the same as in the static case. That is to say, the amount of separated flow was reduced. Hence, it would appear that the reduction

in the amount of separated flow was the primary factor in reducing the magnitudes of the damping-in-yaw and cross derivatives that occurred at high values of α when fences were added to the delta-wing model.

The effect of the fence on $C_{l\beta}$ (fig. 8) is similar to the effect produced by most of the devices used to improve longitudinal stability characteristics such as the incorporation of camber and twist and the use of leading-edge flaps, slats, and chord-extensions. (See refs. 9 to 14.) The linear extension of the $C_{l\beta}$ curve to a higher angle of attack before the break has also been shown to result from an increase in Reynolds number. (See refs. 8, 11, and 15 to 17.) The Reynolds number effect, however, depends on other factors such as leading-edge radius, sweep angle, and roughness. As an example, for a wing having a well-rounded leading edge, an increase in Reynolds number would provide an effect on $C_{l\beta}$ similar to that shown for the effect of fences in figure 8. For a wing with a sharp leading edge, such as that of a biconvex airfoil section, changes in Reynolds number have little influence on the results. In general, therefore, it would appear that a linearization of the $C_{l\beta}$ curve to higher angles of attack or lift coefficients, in any manner involving a reduction in separated flow, would provide reductions in the out-of-phase oscillatory derivatives. Although the results presented herein were obtained for a delta wing, the large magnitudes of the oscillatory derivatives result principally from separated flow due to wing sweep, so that the results should be applicable for other swept-wing plan forms as well.

Effect of Frequency

The effect of oscillation frequency on the derivatives of the delta-wing model with and without a fence for $\alpha = 24^\circ$, and with amplitude of oscillation $\psi_0 = \pm 6^\circ$, is presented in figure 10. The damping-in-yaw and cross-derivative data for the fence-off configuration indicate trends with frequency similar to those shown in references 2 and 4 in that the magnitude of the derivatives increases with decreasing values of reduced frequency. The addition of a fence on each wing semispan provided the largest change in both the out-of-phase and in-phase derivatives at the low values of k . As reduced frequency was increased, the effectiveness of the fence was reduced.

Values for the steady-state condition plotted at $k = 0$ for the directional stability and effective dihedral derivatives were obtained from the static-sideslip data presented in figure 9 for the model mounted on the oscillation strut. The magnitude of the derivatives was determined by using a linear variation over a range of β from -6° to 6° .

Effect of Amplitude

The effect of oscillation amplitude on the derivatives of the delta-wing model with and without a fence is presented in figure 11 for one angle of attack, $\alpha = 24^\circ$, and one frequency of oscillation, $k = 0.0650$. For the fence-off configuration, rather large effects of oscillation amplitude are evident on the out-of-phase derivatives, particularly on $C_{l_{r,\omega}} - C_{l_{\beta,\omega}}$. Reference 4 indicates that even larger amplitude effects exist at lower values of reduced frequency. Addition of wing fences almost eliminated the effect of oscillation amplitude on $C_{n_{r,\omega}} - C_{n_{\beta,\omega}}$ and $C_{l_{r,\omega}} - C_{l_{\beta,\omega}}$ shown for the fence-off configuration apparently by reducing the amount of flow separation on the wing surface. The out-of-phase data of figure 11 show that the influence of the fences on these derivatives increases as oscillation amplitude increases. Fence-on and fence-off results for $C_{n_{\beta,\omega}} + k^2 C_{n_{r,\omega}}$ and $C_{l_{\beta,\omega}} + k^2 C_{l_{r,\omega}}$, however, show identical trends with oscillation amplitude with only the magnitude of the values differing.

Number of Fences

Results for several multiple fence configurations were obtained at several of the higher angles of attack. The data are presented in figure 7 and were discussed previously. However, a clearer indication of the effect on the derivatives of single and double fence configurations and also of fence spanwise location is shown in figure 12 for $\alpha = 24^\circ$. All three fences used to obtain the data were identical, both in fence height and length. For single fences on each wing semispan, data were obtained for the fences located successively at the $0.50b/2$, $0.60b/2$, and $0.70b/2$ spanwise stations. The double fence configuration had one fence located at the $0.35b/2$ station, and the other fence was located successively at the same three outboard stations.

In figure 12, the trends with spanwise location are opposite for single and double fence configurations. Differences between fence-on and fence-off data were larger in all cases for the double fence configuration than for the single fence configuration, except for the value of $C_{l_{\beta,\omega}} + k^2 C_{l_{r,\omega}}$ with the fence at the $0.50b/2$ station. These differences merely indicate that the double fences were more effective than a single fence in reducing or controlling the flow separation on the wing surface. For the single fence configurations, the largest differences between fence-off and fence-on data were obtained for fences located at the $0.50b/2$ station. When the single fences were moved outboard from the $0.50b/2$ station, the trend of the data was toward the

value for fences off. With double fence configurations, exactly the opposite trend was obtained. The limited results presented herein roughly indicate that the maximum fence effectiveness occurred for the single fence configuration when the wing semispan was divided in half and for the double fence configuration when divided into about thirds.

Some Effects of Fence Geometric Characteristics

Some indication of the effect on the oscillatory derivatives at $\alpha = 24^\circ$ of fence height and fence spanwise location is presented in figure 13 for single fence configurations. Values of the derivatives are plotted against the ratio of fence height to wing thickness for configurations involving three different fence heights and four different spanwise locations. Fence lengths varied at each of the different spanwise stations so that the fences covered the wing chord forward of the beveled trailing edge. Results are plotted against the ratio of fence height to wing thickness in figures 14 and 15 for configurations having single fences of various lengths at the $0.50b/2$ and $0.60b/2$ spanwise stations. It should be noted that, for the fences used in this investigation, an increase in fence height also resulted in an increase in the fence overhang at the wing leading edge.

The results of figures 13, 14, and 15 for effective dihedral, damping-in-yaw, and cross derivatives indicate that the effectiveness of the fence increases as fence height increases when single fences are located at the $0.50b/2$ and $0.60b/2$ stations. The variation with fence height for fences at the $0.35b/2$ and $0.70b/2$ stations, however, is not as consistent as for fences at the $0.50b/2$ and $0.60b/2$ stations. Of particular interest in figures 13, 14, and 15 is the variation of directional stability with fence height. For the small-height fences tested ($\frac{h}{t} = 0.33$), it appears that the addition of the fence caused a reduction in the model directional stability except for the one configuration with the fence located at the $0.35b/2$ station. The effect of fence length as shown in figures 14 and 15 appears to be less important than fence height and spanwise location, at least for the two spanwise stations investigated. This might have been anticipated since the type of flow separation experienced on this delta-wing model is of the leading-edge variety. (See ref. 9.) In general, the results show that differences in fence geometric characteristics can result in fairly large differences in the values of the derivatives.

SUMMARY OF RESULTS

From a wind-tunnel investigation made at low speed to determine some of the effects of wing fences on the lateral stability derivatives of a 60° delta-wing model oscillating continuously in yaw, the following observations can be made:

1. The addition of wing fences provided large reductions in the magnitudes of the out-of-phase derivatives, that is, the damping-in-yaw derivative $C_{n_{r,\omega}} - C_{n_{\dot{\beta},\omega}}$ and cross (rolling moment due to yawing) derivative

$C_{l_{r,\omega}} - C_{l_{\dot{\beta},\omega}}$, at high angles of attack and low reduced frequency by reducing the amount of separated flow on the wing surface. These reductions were significant in that the derivatives for the basic wing at high angles of attack were several times as large as the corresponding derivatives for some complete models at low angles of attack. In addition, increases were obtained in the magnitudes of the in-phase derivatives, the directional stability $C_{n_{\beta,\omega}} + k^2 C_{n_{r,\omega}}$ and effective dihedral $C_{l_{\beta,\omega}} + k^2 C_{l_{r,\omega}}$, such that the values of the derivatives for the model with fences on more nearly approached the theoretical values for this plan form in unseparated flow. In the low-angle-of-attack range, the addition of wing fences did not change the values of the in-phase or out-of-phase derivatives.

2. Increases in Reynolds number and the use of various devices commonly employed to improve the longitudinal stability characteristics such as camber, twist, and leading-edge flaps and slats may provide changes in the oscillatory derivatives similar to the changes produced by wing fences.

3. At high angles of attack, the addition of wing fences considerably reduced the variation of the out-of-phase derivatives with oscillation amplitude and reduced frequency. The fence effectiveness increased with an increase in oscillation amplitude and with decreasing values of reduced-frequency parameter.

4. Differences in fence geometric characteristics and the number of fences used resulted in fairly large differences in the values of the derivatives.

Langley Aeronautical Laboratory,
National Advisory Committee for Aeronautics,
Langley Field, Va., April 3, 1956.





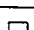
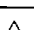


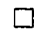





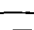
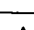






REFERENCES

1. Riley, Donald R., Bird, John D., and Fisher, Lewis R.: Experimental Determination of the Aerodynamic Derivatives Arising From Acceleration in Sideslip for a Triangular, a Swept, and an Unswept Wing. NACA RM L55A07, 1955.
2. Campbell, John P., Johnson, Joseph L., Jr., and Hewes, Donald E.: Low-Speed Study of the Effect of Frequency on the Stability Derivatives of Wings Oscillating in Yaw With Particular Reference to High Angle-of-Attack Conditions. NACA RM L55H05, 1955.
3. Queijo, M. J., Fletcher, Herman S., Marple, C. G., and Hughes, F. M.: Preliminary Measurements of the Aerodynamic Yawing Derivatives of a Triangular, a Swept, and an Unswept Wing Performing Pure Yawing Oscillations, With a Description of the Instrumentation Employed. NACA RM L55L14, 1956.
4. Fisher, Lewis R.: Experimental Determination of the Effects of Frequency and Amplitude on the Lateral Stability Derivatives for a Delta, a Swept, and an Unswept Wing Oscillating in Yaw. NACA RM L56A19, 1956.
5. Runyan, Harry L., Woolston, Donald S., and Rainey, A. Gerald: Theoretical and Experimental Investigation of the Effect of Tunnel Walls on the Forces on an Oscillating Airfoil in Two-Dimensional Subsonic Compressible Flow. NACA TN 3416, 1955. (Supersedes NACA RM L52L17a.)
6. Campbell, John P., and Woodling, Carroll H.: Calculated Effects of the Lateral Acceleration Derivatives on the Dynamic Lateral Stability of a Delta-Wing Airplane. NACA RM L54K26, 1955.
7. Bird, John D., and Riley, Donald R.: Some Experiments on Visualization of Flow Fields Behind Low-Aspect-Ratio Wings by Means of a Tuft Grid. NACA TN 2674, 1952.
8. Polhamus Edward C., and Sleeman, William C., Jr.: The Rolling Moment Due to Sideslip of Swept Wings at Subsonic and Transonic Speeds. NACA RM L54L01, 1955.
9. Furlong, G. Chester, and McHugh, James G.: A Summary and Analysis of the Low-Speed Longitudinal Characteristics of Swept Wings at High Reynolds Number. NACA RM L52D16, 1952.

10. Jaquet, Byron M.: Effect of Linear Spanwise Variations of Twist and Circular-Arc Camber on Low-Speed Static Stability, Rolling, and Yawing Characteristics of a 45° Sweptback Wing of Aspect Ratio 4 and Taper Ratio 0.6. NACA TN 2775, 1952.
11. Griner, Roland F.: Static Lateral Stability Characteristics of an Airplane Model Having a 47.7° Sweptback Wing of Aspect Ratio 6 and the Contribution of Various Model Components at a Reynolds Number of 4.45×10^6 . NACA RM L53G09, 1953.
12. Queijo, M. J., and Wolhart, Walter D.: Experimental Investigation of the Effect of Vertical-Tail Size and Length and of Fuselage Shape and Length on the Static Lateral Stability Characteristics of a Model With 45° Sweptback Wing and Tail Surfaces. NACA Rep. 1049, 1951. (Supersedes NACA TN 2168.)
13. Jaquet, Byron M., and Brewer, Jack D.: Low-Speed Static-Stability and Rolling Characteristics of Low-Aspect-Ratio Wings of Triangular and Modified Triangular Plan Forms. NACA RM L8L29, 1949.
14. Letko, William, and Jaquet, Byron M.: Effect of Airfoil Profile of Symmetrical Sections on the Low-Speed Static-Stability and Yawing Derivatives of 45° Sweptback Wing Models of Aspect Ratio 2.61. NACA RM L8H10, 1948.
15. Neely, Robert H., and Conner, D. William: Aerodynamic Characteristics of a 42° Sweptback Wing With Aspect Ratio 4 and NACA 64₁-112 Airfoil Sections at Reynolds Numbers From 1,700,000 to 9,500,000. NACA RM L7D14, 1947.
16. Salmi, Reino J.: Yaw Characteristics of a 52° Sweptback Wing of NACA 64₁-112 Section With a Fuselage and With Leading-Edge and Split Flaps at Reynolds Numbers From 1.93×10^6 to 6.00×10^6 . NACA RM L8H12, 1948.
17. Campbell, John P., and Toll, Thomas A.: Factors Affecting Lateral Stability and Controllability. NACA RM L8A28a, 1948.

TABLE I

SUMMARY OF FENCE ON OSCILLATION TESTS

Test conditions			Fence configuration				Figure	Symbol
α , deg	ψ_0 , deg	k	Fences per semispan	$\frac{y}{b/2}$, ft	h/t, in.	X, in.		
24	± 6	0.0650	1	0.35	0.33, .66, 1.00	15.99	13	
				.50	.33, .66, 1.00	11.31	13, 14	
					.33, .66, 1.00	8.19	14	
					.33	5.07	14	
					.66		12, 14	 
					1.00		14	
				.60	.33, .66, 1.00	8.19	13, 15	 
					.33	5.07	15	
					.66		12, 15	 
					1.00		15	
				.70	.33	5.07	13	
					.66		12, 13	 
					1.00		13	
24	(b)	.0650	1	.50	.66	5.07	11	
24	± 6	(c)					10	
(a)	± 6	.0650					7	
24	± 6	.0650	2	.35, .50	.66	5.07	12	
			2	.35, .60				
			2	.35, .70				
30	± 6	.0650	2	.35	.66	5.07	7	
				.70	1.00			
24, 26, 28, 30	± 6	.0650	2	.35, .70	.66	5.07	7	
24, 26, 28, 30	± 6	.0650	3	.35, .50	.66	5.07	7	
				.70	1.00			

^aRange of α : 0, 4, 8, 12, 16, 18, 20, 22, 24, 26, 28, 30.^bRange of ψ_0 : ± 2 , ± 4 , ± 6 , ± 8 , and ± 10 .^cRange of k: 0.0325, 0.0650, 0.0975, 0.1300, and 0.1950.

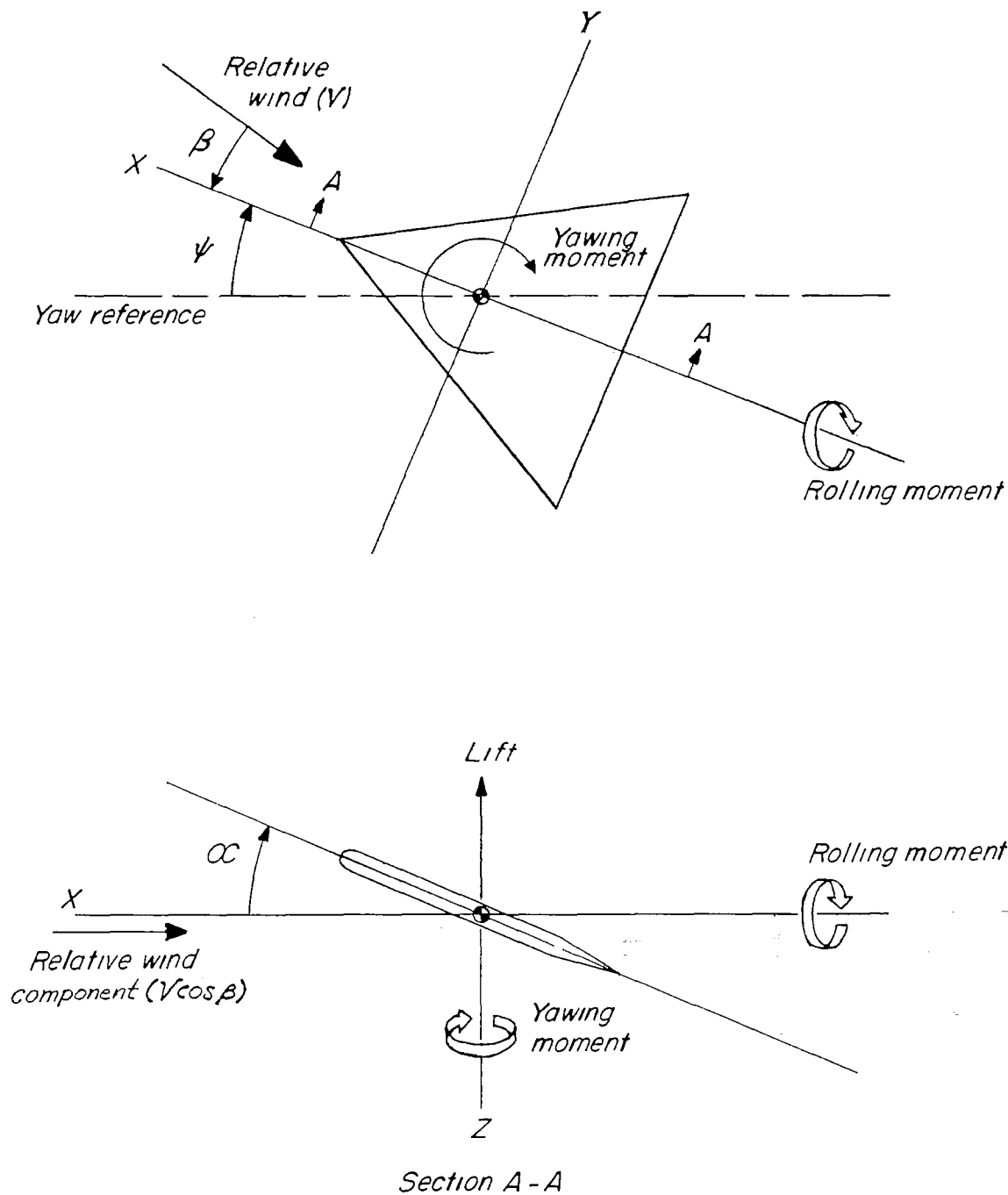
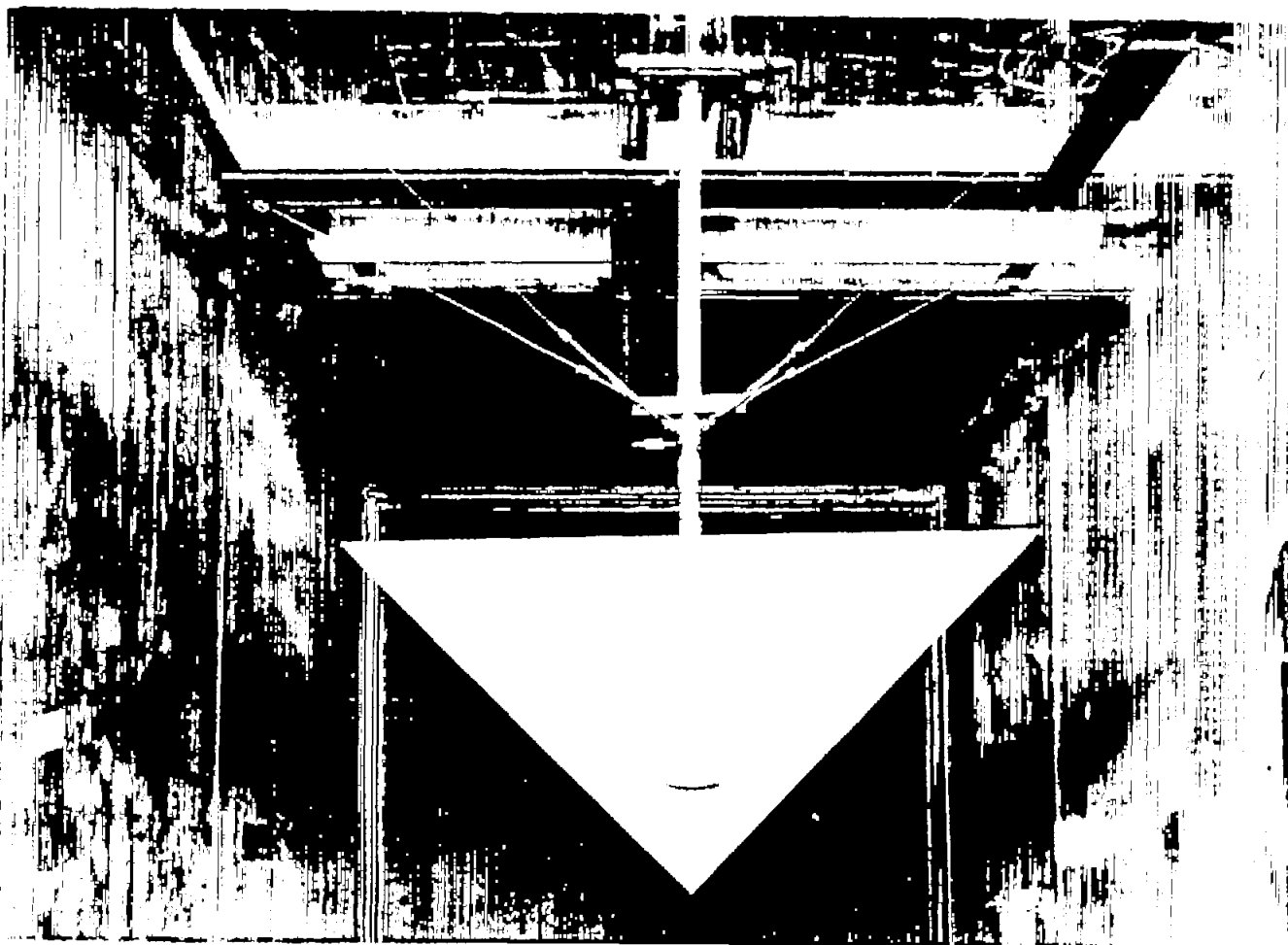
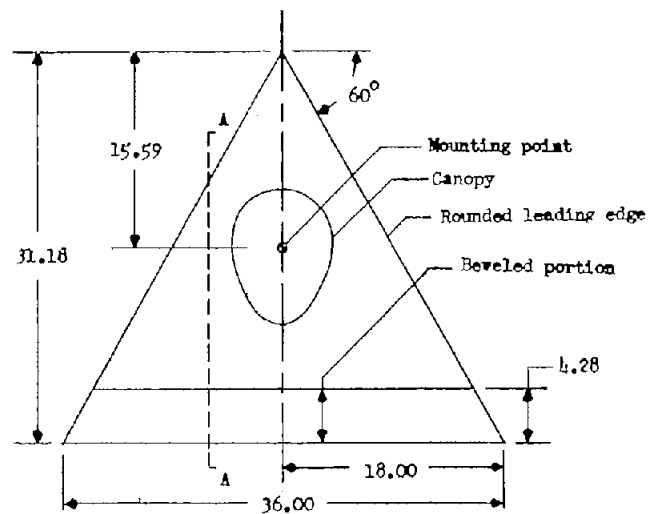


Figure 1.- Sketch of axes used. Arrows indicate positive directions of moments and angular displacements. Yaw reference is generally chosen to coincide with initial relative wind.



L-90948

Figure 2.- Rear view of 60° delta wing with canopy at an angle of attack and mounted on the oscillation strut in the 6- by 6-foot test section of the Langley stability tunnel.



Section A-A

Aspect ratio	2.31
Leading edge sweep angle, deg ...	60
Dihedral angle, deg	0
Twist, deg	0
Airfoil section	Flat plate
Area, sq. ft.	3.90
Span, ft.	3.00
Mean aerodynamic chord, ft.	1.73

Figure 3.- Details of 60° delta-wing model.
All dimensions are in inches.

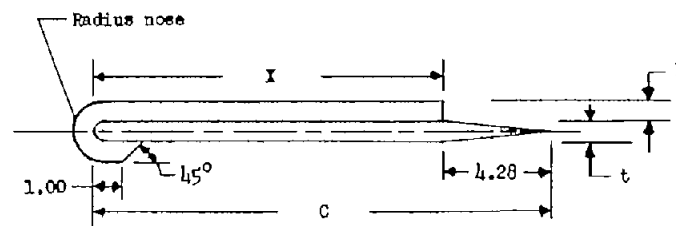
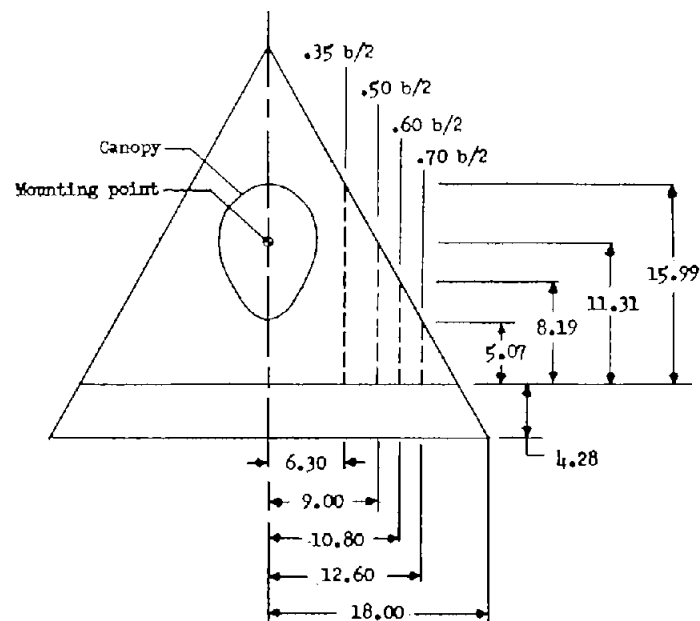


Figure 4.- Sketch of fence shape and spanwise
fence locations used. All dimensions are
in inches.

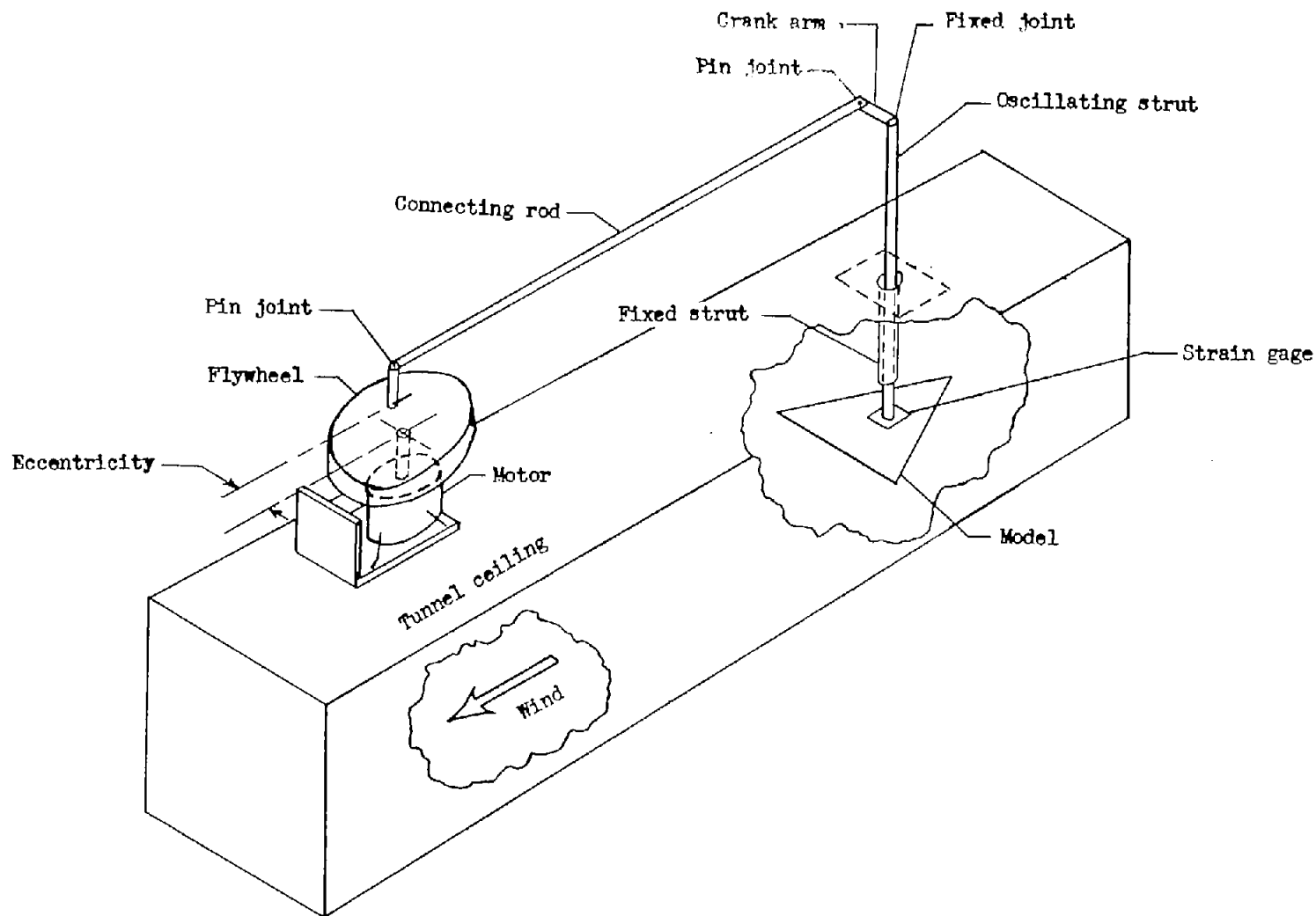


Figure 5.- Schematic sketch of oscillation-in-yaw equipment.

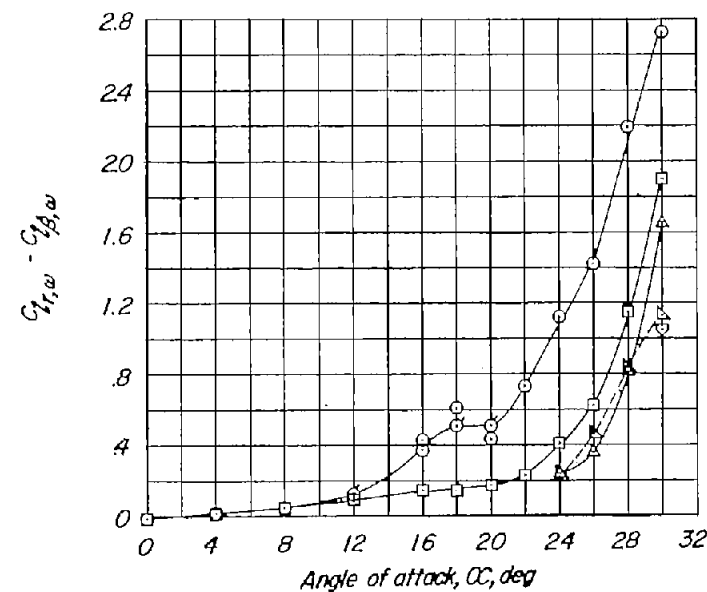
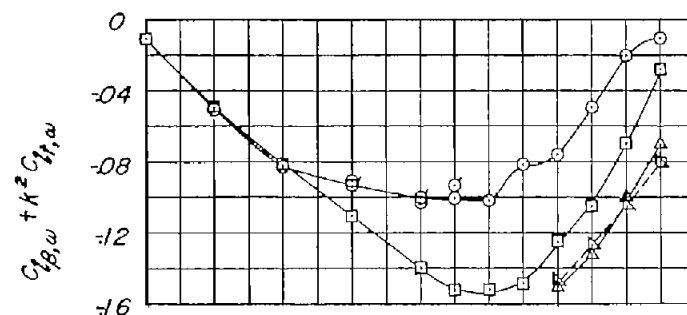
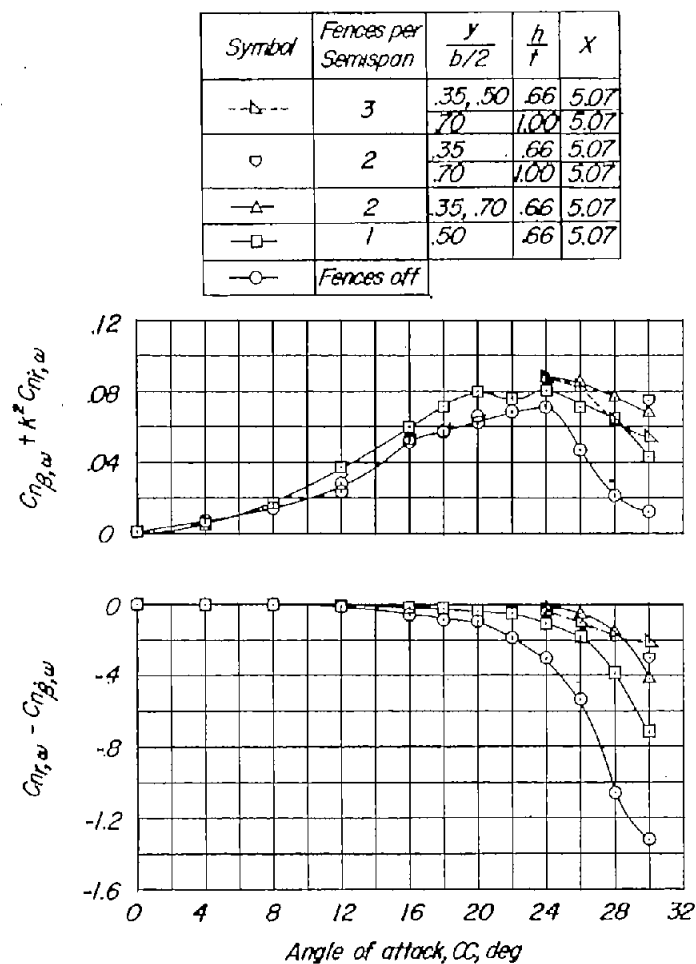
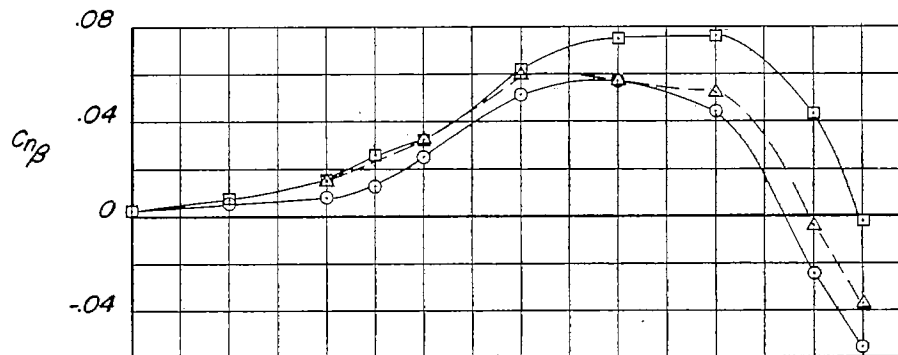


Figure 7.- Variation of the oscillatory derivatives with angle of attack for the 60° delta-wing model without and with several fence configurations. $k = 0.0650$; $\psi_0 = \pm 6^\circ$; flagged symbols represent check points.



Symbols	Fences per Semispan	$\frac{y}{b/2}$	$\frac{h}{t}$	X
△	1	.50	.33	5.07
□	1	.50	.66	5.07
○	Fences off			

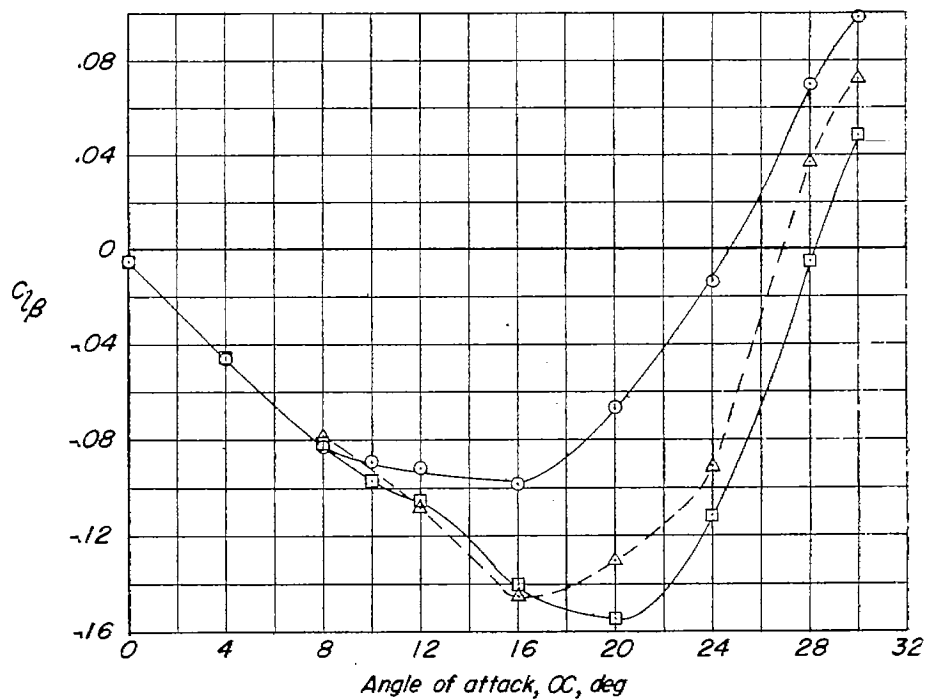


Figure 8.- Variation of static-sideslip derivatives $C_{n\beta}$ and $C_{l\beta}$ with angle of attack for 60° delta-wing model with and without fences. Model is mounted on a conventional single strut support with a streamlined fairing present. Slopes are obtained from test data at β of -6° and 6° .

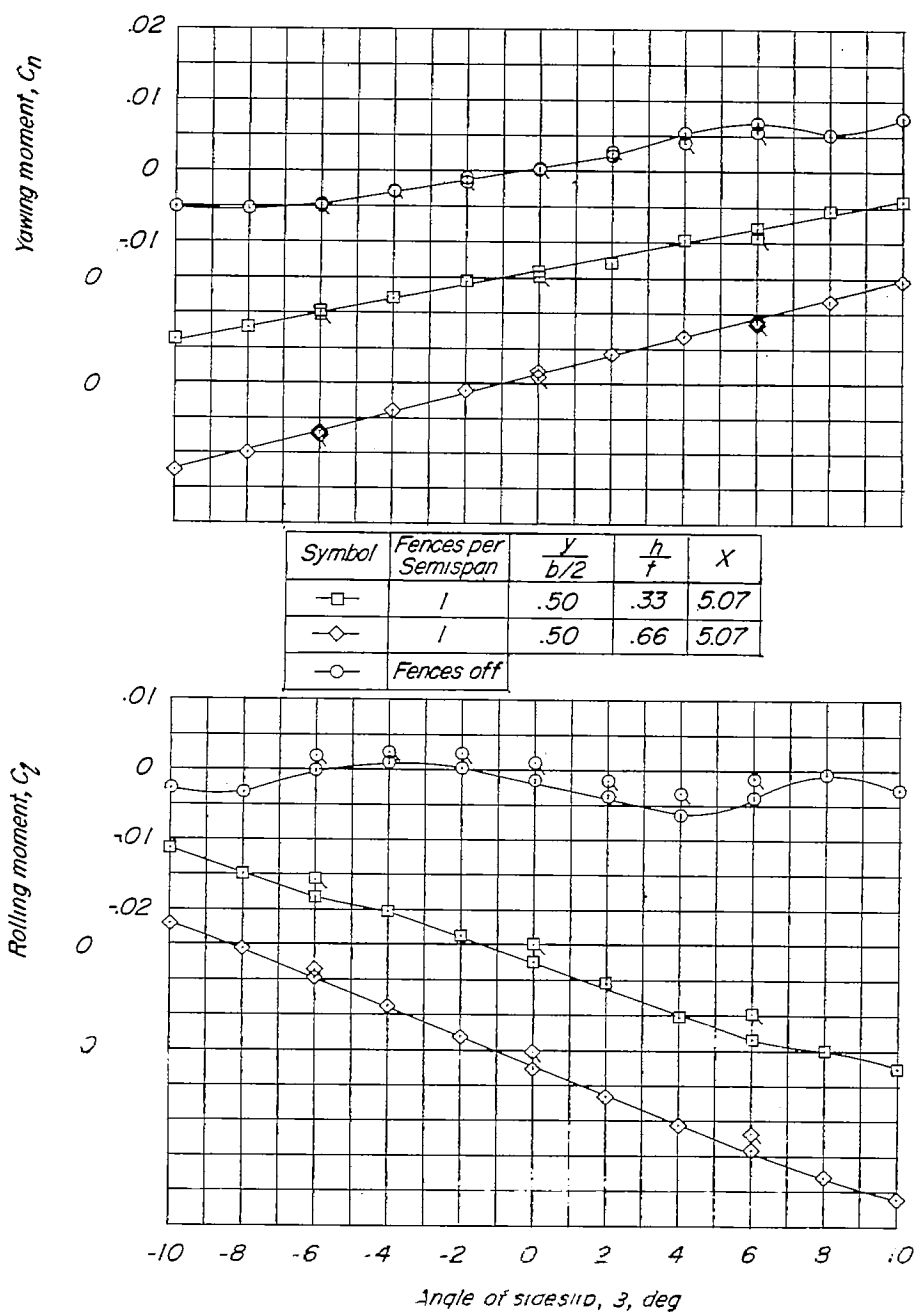


Figure 2.- Variation of static rolling- and yawing-moment coefficients with sideslip angle for the 60° delta-wing model with and without fences at $\alpha = 24^\circ$. Plain symbols represent data for model mounted on oscillation strut; and tailed symbols, for model on conventional single support strut with a streamlined fairing present.

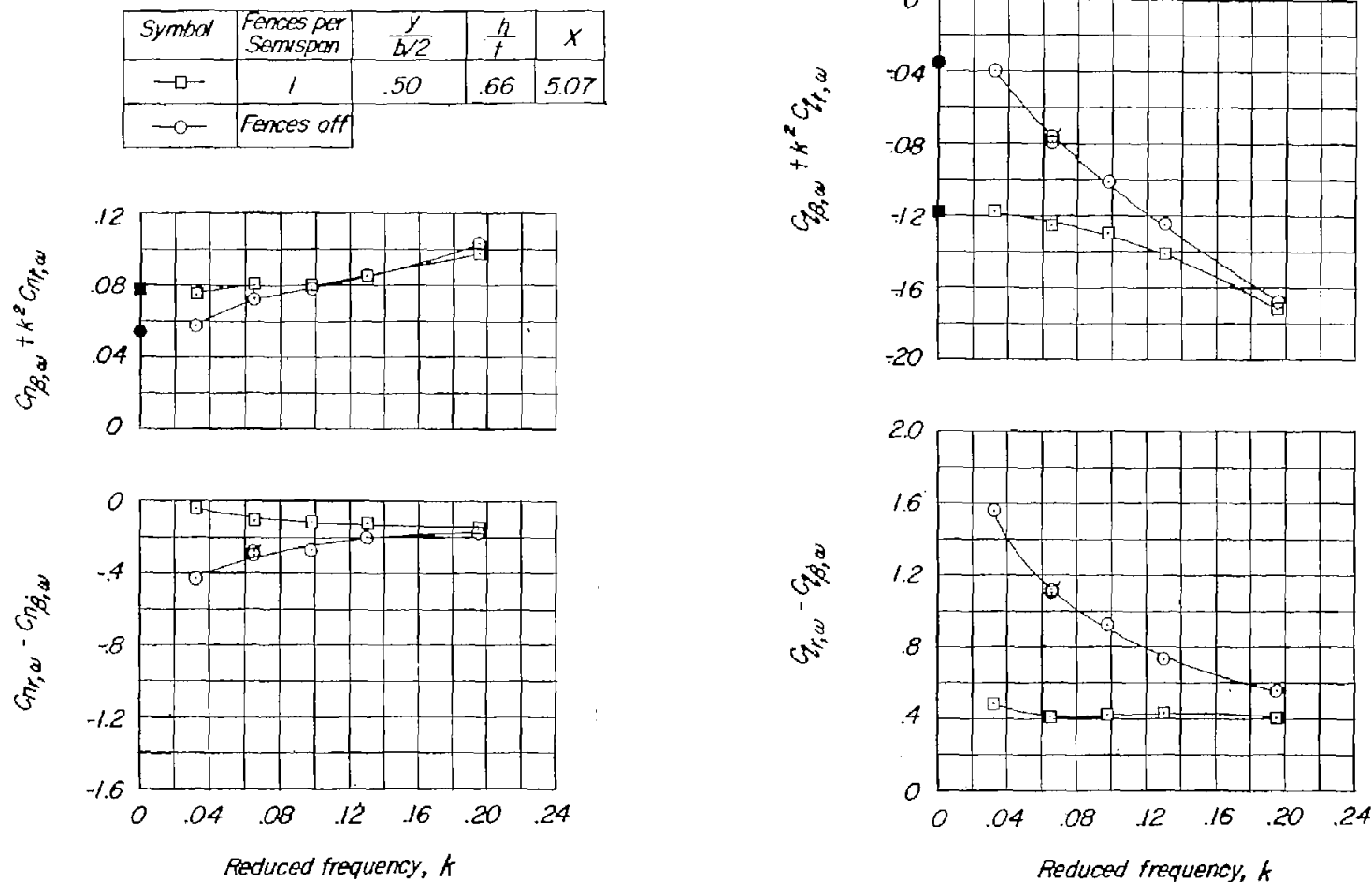


Figure 10.- Effect of oscillation frequency on oscillatory derivatives of 60° delta-wing model with and without a fence. $\alpha = 24^\circ$; $\psi_0 = \pm 6^\circ$; flagged symbols represent check points.

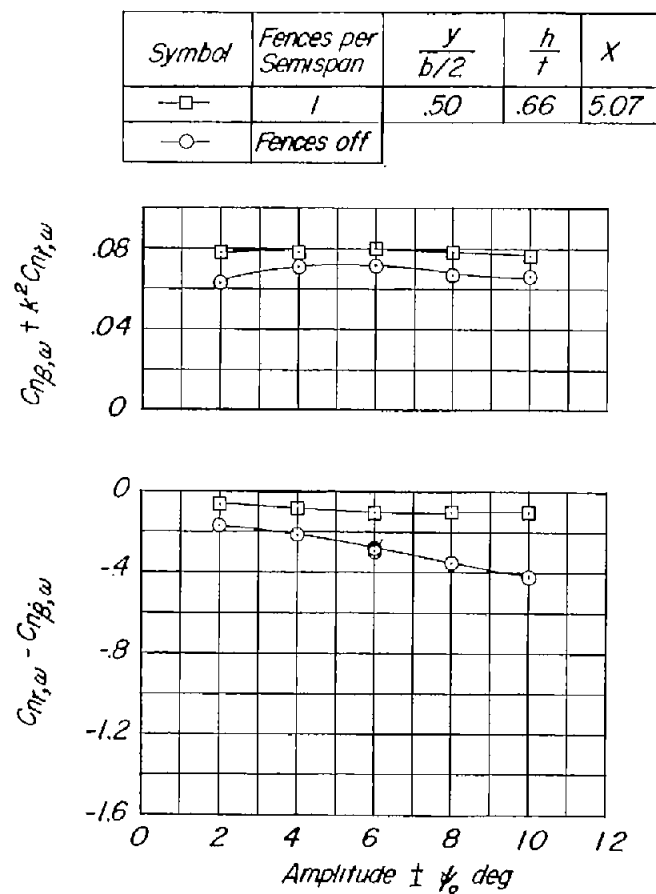
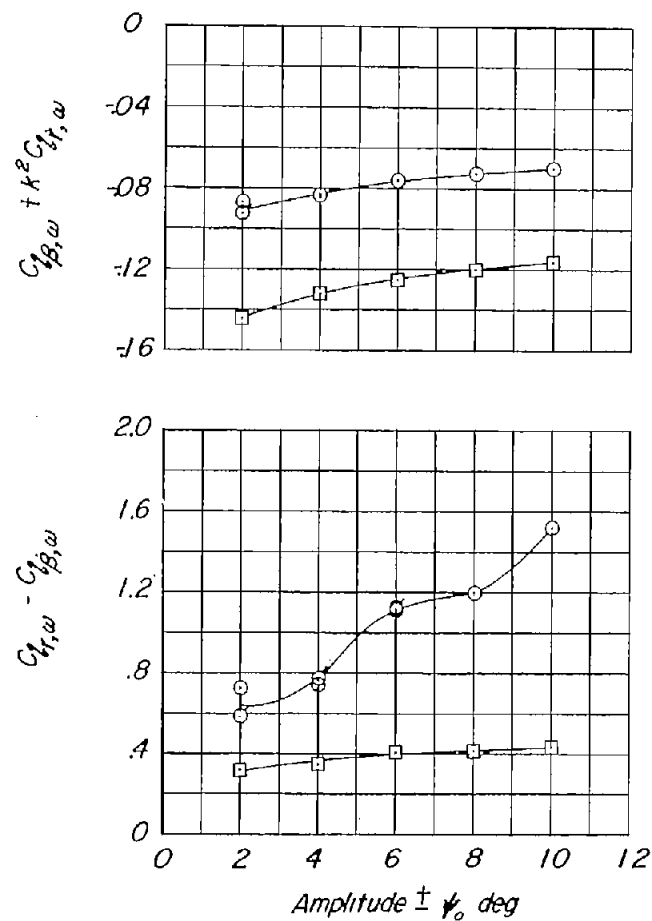


Figure 11.- Effect of oscillation amplitude on oscillatory derivatives of 60° delta-wing model with and without a fence. $\alpha = 24^\circ$; $k = 0.0650$; flagged symbols represent check points.



Symbol	Fences per Semispan	$\frac{y}{b/2}$	$\frac{h}{t}$	X
—□—	1	.50, .60 or .70	.66	5.07
—◇—	2	.35 .50, .60 or .70	.66	5.07
----	Fences off			

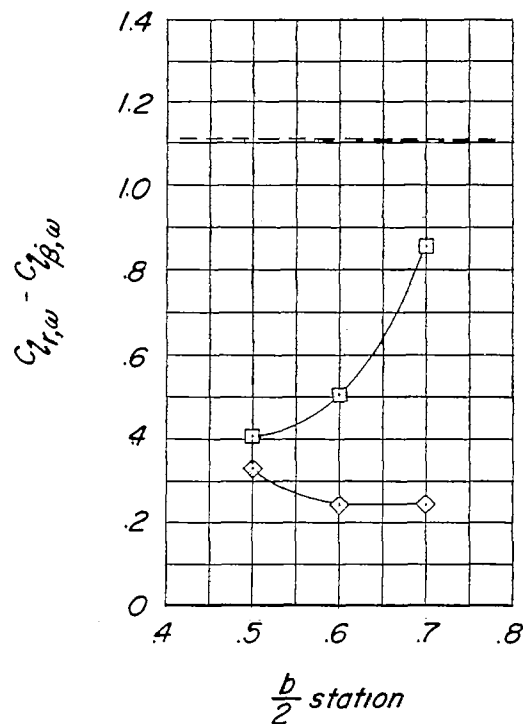
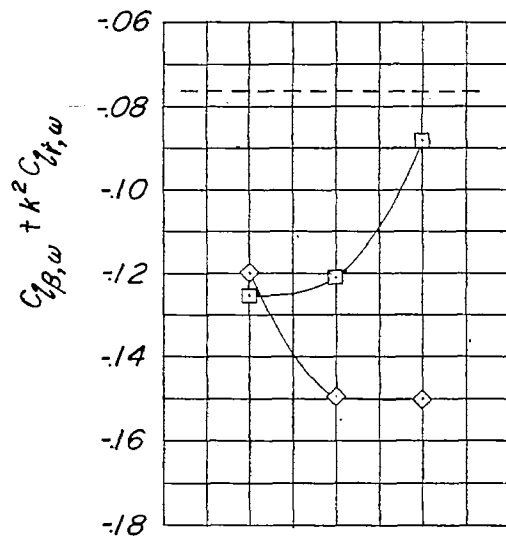
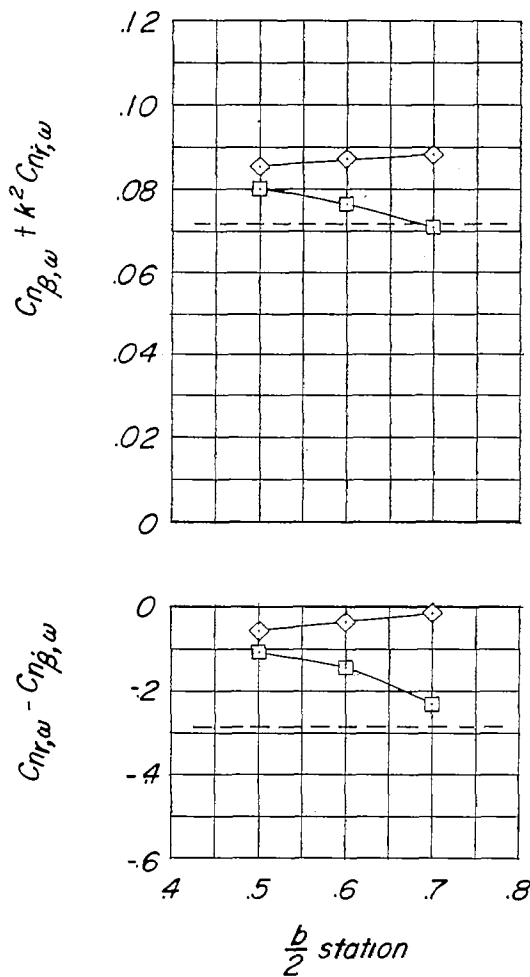


Figure 12.- Effect on oscillatory derivatives of single and double fences per semispan and of fence spanwise location. $\alpha = 24^\circ$; $k = 0.0650$; $\psi_0 = \pm 6^\circ$.

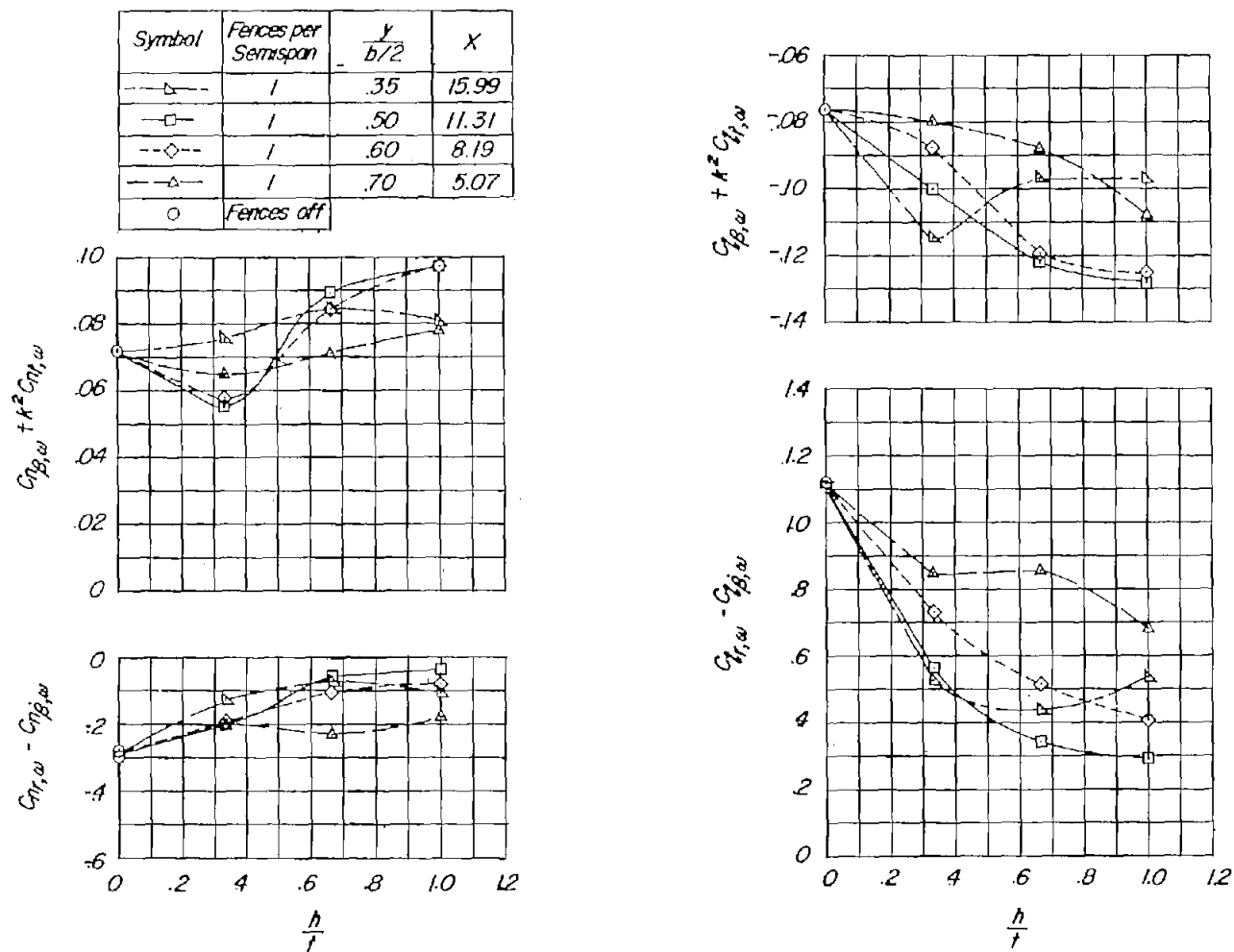


Figure 13.- Effect on oscillatory derivatives of fence spanwise location and height for fences covering the wing chord forward of the beveled trailing edge and for a single fence located on each wing semispan. $\alpha = 24^\circ$; $k = 0.0650$; $\psi_0 = \pm 6^\circ$.

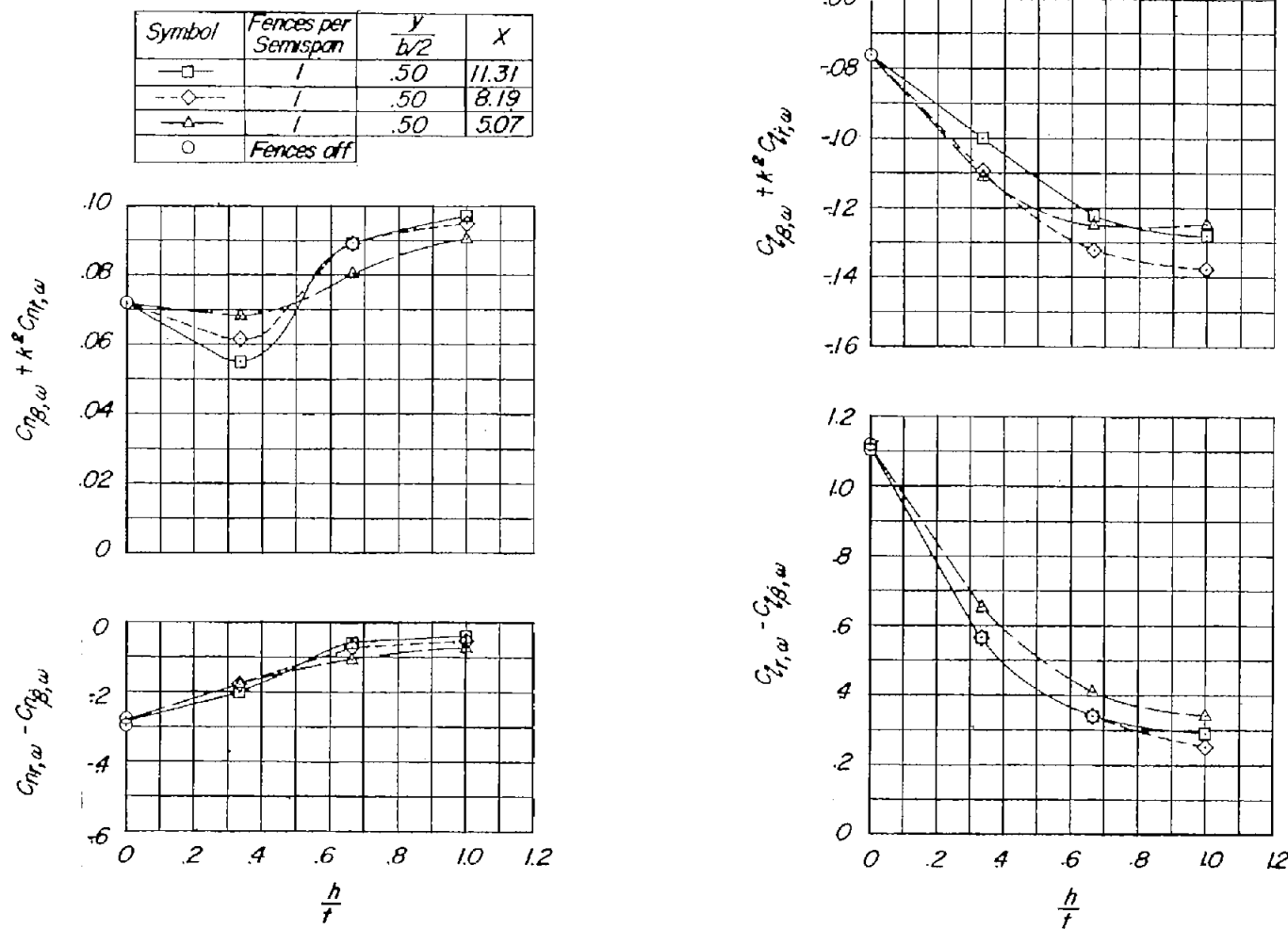


Figure 14.- Effect on oscillatory derivatives of fence length and height for a single fence located on each wing semispan at the $0.50b/2$ station. $\alpha = 24^\circ$; $k = 0.0650$; $\psi_0 = \pm 6^\circ$.

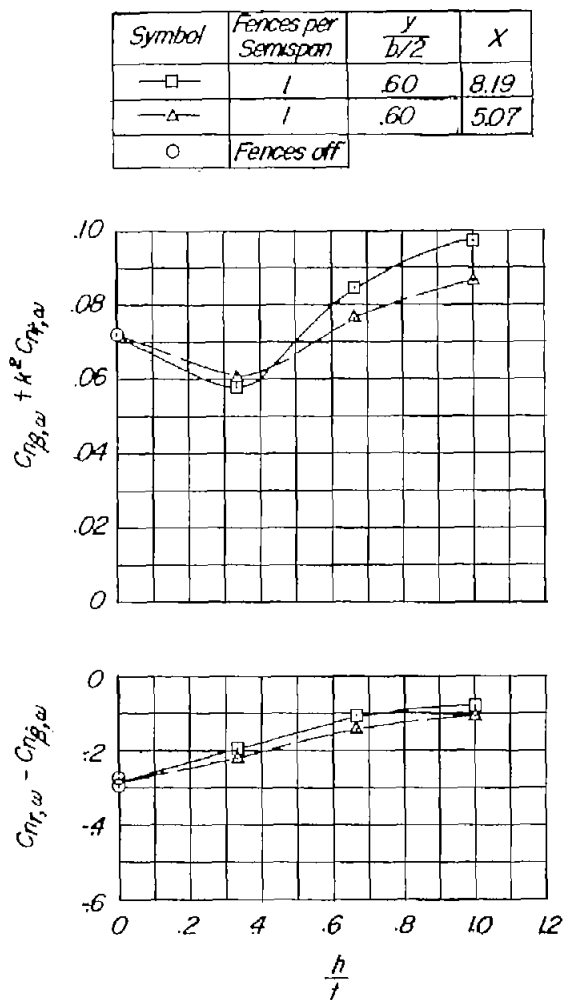


Figure 15.- Effect on oscillatory derivatives of fence length and height for a single fence located on each wing semispan at the $0.60b/2$ station. $\alpha = 24^\circ$; $k = 0.0650$; $\psi_0 = 16^\circ$.

